A&A manuscript no.
(will be inserted by hand later)

Your thesaurus codes are:
02(02.01.2; 08.09.2 Her X-1; 13.25.5)

ASTRONOMY
AND
ASTROPHYSICS
7.9.1995

Her X-1: Modelling the Anomalous and Preeclipse Dips with the Coronal Wind Model

S. Schandl⋆

Max-Planck-Institut für Astrophysik, Karl Schwarzschildstr. 1, 85740 Garching, Germany

Received date; accepted date

Abstract. The interaction between the accretion stream and the thin, tilted and twisted accretion disk is found to be consistent with the observed complex dip structure in the X-ray signal of Her X-1.

The stream falls into the warped disk mostly from above or below where the hydrodynamic interaction leads to a cold clumpy spray covering the X-ray source once per orbit. We test this model with the warped disk shape obtained from coronal wind torques and get the correct phases for the observed preeclipse dips. This includes the peculiar "marching backwards" in orbital phase with the proceeding 35 day period.

The penetration of the stream further results in a turbulent thickening of the disk rings at the involved radii which last for the dynamical timescale which is of the order of the Kepler period. At turn-on the observer looks marginally over a particular region of the disk surface. Now, at orbital phases where this is thickened, it will cover the X-ray source again producing an anomalous dip. Later in the 35 day period the observer looks far over the disk and its temporal thickening. This occurs twice per orbit and the simulated phases agree with the observed times. – Because these dips and the turn-on are both caused by the disk the turn-on always takes place at the same orbital phases reproducing the observations.

Key words: accretion disks – stars: Her X-1 – X-rays: stars

1. Introduction

The X-ray binary HZ Her/Her X-1 consists of a $2.2M_\odot$ Roche lobe filling companion and an accreting magnetic neutron star. Besides the 1.24 sec spin period of Her X-1 and the 1.7 day orbit the binary shows a longperiodic behaviour on a timescale of 35 days. The great variety of observations and theories grown up around it are reviewed e.g. by Priedhorsky & Holt (1987) or recently by Choi et al. (1994). Table 1 summarizes some system parameters.

Restricting to the longperiodic behaviour of the X-rays the 35 day cycle begins with a rapid rise of the signal, the turn-on, combined with cold matter absorption features in the X-ray spectrum (Becker et al. 1977, Pravdo et al. 1979). At the end of the main-on after about 11 days (turn-off) the signal has dropped down slowly combined with no spectral changes. Later the signal rises again for about one week but the intensity is clearly less than during main-on (Jones & Forman 1976). Afterwards the intensity drops down again until a new cycle starts.

This behaviour is understood in terms of a tilted and twisted accretion disk which the observer on earth sees nearly edge on, because the inclination of the system is very high ($> 80°$) (Gerend & Boynton 1976). A warped disk precesses in the tidal field of the companion (Katz 1973) where the calculated precession period agrees with the observed 35 day period.

The region of the disk which rises above the orbital plane by more than the inclination therefore covers the central X-ray source temporarily during the precession. Additionally there exists a X-ray induced corona which reduces the intensity at the end of the main-on where its optically thick part covers Her X-1. This corona produces also the weak unmodulated radiation in the low state just before turn-on (Becker et al. 1977, Pravdo et al. 1979) and during the dips (see below) via scattering (Jones & Forman 1976, Davison & Fabian 1977). At turn-off the unpulsed component decreases slower than the direct pulsed fraction suggesting an extended scattering region as the corona is.

Our coronal wind model (Schandl & Meyer 1994) reproduces this corona which is optically thick at small radii ($r \leq 10^{10}$ cm) and which temporarily covers the central neutron star because the inner region of the disk is tilted. Because of the disk twist the covering by the inner corona and the outer disk region occur at different phases of the 35 day cycle. Thus we can observe the X-ray source twice: The disk itself opens the view at the beginning of the main-on, the corona crosses the line of sight at its end. At the short-on it is the other way around though the corona remains partially in front of Her X-1.

Additionally to the longperiodic variation and the eclipses by the companion on the orbital period of 1.7 days the X-ray in-

⋆ email: suh@mpa-garching.mpg.de

Table 1. Parameters of the X-ray binary HZ Her/Her X-1

Parameters of the system HZ Her/Her X-1				**reference**
orbital period	$P_{\rm orb}$	=	1.7 d	1
orbital period change	$\dot{P}_{\rm orb}/P_{\rm orb}$	=	$-1.3 \cdot 10^{-8}$ yr^{-1}	2
binary separation	a	=	$6 \cdot 10^{11}$ cm	3
eccentricity of the orbit	e	=	$3 \cdot 10^{-4}$	3
inclination of the system	i	=	$80^\circ - 90^\circ$	3,4,5
mass of the companion	$M_{\rm HZ}$	=	$2.2\,M_\odot$	3,4
mass of the neutron star	$M_{\rm n\star}$	=	$1.3\,M_\odot$	3,4
spin period of the neutron star	$P_{\rm spin}$	=	1.24 sec	1
X-ray luminosity	L	=	$10^{37.3}$ erg sec^{-1}	6
magnetic field strength of the neutron star	B	=	$10^{12.7}$ Gauß	7,8
precession period of the disk	$P_{\rm prec}$	=	35 d	9
disk radius	$r_{\rm a}$	=	$1 - 2 \cdot 10^{11}$ cm	10,11,12
inclination of the system	i	=	81.5°	13
accretion rate of the neutron star	$\dot{M}_{\rm acc}$	=	$10^{17.3}$ g/sec	13
mass flow in the accretion stream	$\dot{M}_{\rm s}$	=	$10^{17.9}$ g/sec	13
disk radius	$r_{\rm a}$	=	$1.7 \cdot 10^{11}$ cm	13

References: 1 Tananbaum et al. 1972, 2 Deeter et al. 1991, 3 Deeter et al. 1981, 4 Middleditch & Nelson 1976, 5 Gerend & Boynton 1976, 6 McCray et al. 1982, 7 Trümper et al. 1978, 8 Pravdo et al. 1977, 9 Giacconi et al. 1973, 10 Oke 1976, 11 Crosa & Boynton 1980, 12 Middleditch 1983, 13 quantities in our model

tensity undergoes two types of dips (Giacconi et al. 1973). The *preeclipse dips* occur just before the eclipses and march backwards in orbital phase as the 35 day cycle proceeds. They last for 2 to 5 hours and show strong variations on short timescales of the intensity, the spectrum and the pulse shape. An unabsorbed, unpulsed component at a few percent of the high state level suggests itself to be scattered by the hot corona (Choi et al. 1994, Reynolds & Parmar, in press).

The other type of dips are the *anomalous dips* which occur only just after turn-on at orbital phases around 0.2 or 0.7. These are the same phases where the turn-on itself takes place. (Giacconi et al. 1973). The anomalous dips are somewhat shorter, 1 to 2 hours, but show cold matter absorption features in the spectrum, too. (Reynolds & Parmar, in press).

In terms of the periodic mass transfer model Crosa & Boynton (1980) and Boynton et al. (1980) described the dips as to be caused by matter deposited at the disk rim at times of mass transfer. The blobs Choi et al. (1994) described to be generated at the hot spot covering the X-ray source are placed at the disk rim, too. – We propose here a new model for the dips that is based on the shape of the disk as predicted by our model of the coronal wind torques and supported by the observations.

1.1. The dips in terms of the coronal wind model

Considering the interaction of the accretion stream and the thin, warped disk we find that the stream which falls in the orbital plane hits the disk mostly from above or below and not at the rim. The angle between the stream and the disk surface are very small and thus the impact is moderate enough that the stream does not go through the disk. But of course the free fall velocity of the stream is highly supersonic and the Keplerian velocity of the disk matter running against the penetrating stream is highly supersonic, too. Therefore the impact causes shock waves.

The matter running through the shock fronts gets refracted because only the velocity component perpendicular to the front gets reduced to subsonic values. Although we have to discuss the influence of cooling on this event the refracting properties of shocks are a general feature. In particular, some of the matter at the surface of the accretion disk that impacts the penetrating obstacle will get refracted upwards resulting in a cold and clumpy spray spreading above the disk surface. When this gets in front of the X-ray source it will reduce the signal in the way of the preeclipse dips. We will simulate the occurrence times of this spray covering the source and will find a very good agreement with the observed preeclipse dips including their marching backwards in time. An estimation of the mass flow in the spray will show that only a few percent of the disk and stream matter involved into the shocks are necessary to reproduce the observed column densities.

Otherwise the penetration and break-up of the accretion stream results in heating, turbulent motion and an addition of matter to the disk. All this produces in a thickening of the disk. It gets gradually smoothed out by viscosity and thermal conductivity on a timescale which is comparable to the Keplerian orbital period. Therefore the thickening settles down until the disk matter runs again through the turbulent impact region creating a saw-tooth profile of the disk thickness over orbital phase. – At turn-on the disk opens the line of sight to the central X-ray source. This means the observer looks marginally over the disk surface. More precisely it is the surface at a special disk radius doing the turn-on, because of the twist of the disk. And it is this disk ring which we look marginally over and on which our view depends very sensitively. If this disk ring undergoes the thickening it will cover the X-ray source doing an anomalous dip. This occurs only at turn-on, because we look afterwards far above the disk and its thickened region. And it may occur at two distinct orbital phases because the special disk ring gets impacted twice per orbit, once from above, once from below with a synodic orbital phase difference of about 0.5. The simulated occurrence times will agree with the observed times. The estimated increase of the disk thickness is large enough to reproduce the anomalous dips.

This raises the question of the orbital phases of the turn-on itself. The appearance at the same phases as the anomalous dips indicates a connection between them. In our model the turn-on becomes something like a 'zeroth dip'. Assuming an extended accretion stream the special disk ring gets impacted for a long time doing some thickening. Of course this is maximal when the stream center penetrates into this ring. Just afterwards the stream hits only the innermost disk region giving the view free unrestrictedly (see Fig. 5). If at this moment the disk surface lies above the line of sight to the neutron star it will cover it for another half period because soon afterwards the swelling starts again. But if the now undisturbed disk surface lies under the line of sight the turn-on occurs. Half an orbit later only the strong thickening by the stream center is able to cover the X-ray source once again producing an anomalous dip.

In the following I first give a short description of our coronal wind model (section 2) and the relevant features of the resulting geometrical disk structure (section 3). In section 4 the stream/disk interaction is investigated. Section 5 discusses the origin of the spray and the resulting preeclipse dips and section 6 gives a similar account of the disk thickening and the anomalous dip feature. Section 7 contains the conclusions.

2. The coronal wind model

The X-rays strike the accretion disk surface and generate a hot corona (Shakura & Sunyaev 1973). Its density is proportional to the irradiating flux which depends on the radiation transport in the corona. For a flat disk we simulated the irradiation to be about 3% of the direct X-ray flux of the neutron star (Schandl & Meyer 1994). (Note that the corona is optically thick in radial direction only at small radii ($r < 10^{10}$ cm) where the disk is tilted but not warped. The warping coronal wind occurs at radii $r > 10^{10.2}$ cm.) Because the Compton effect is the main heating and cooling process in the upper layer of the corona and the spectrum is hard enough that the inner energy exeeds the gravitational potential at the outer regions coronal gas leaves the system forming a coronal wind (Begelman et al. 1983). The angular momentum of the gas flow gets lost from the system, too. This loss of mass and angular momentum leads to shrinkage of the orbit and a corresponding period change. Deeter et al. (1991) observed it to be $\dot{\mathrm{P}}/\mathrm{P} = (-1.32 \pm 0.16)\, 10^{-8}\, \mathrm{yr}^{-1}$. Assuming that the coronal wind is the only mass loss from the system and that the companion fills its Roche lobe this observation corresponds to a wind rate of about $10^{17.8}$ g/sec which is three times the accretion rate of the central neutron star. Simulating the coronal wind in detail this amount of mass loss is reproduced by our model very well.

We can describe the accretion disk as consisting of concentric rings and integrate the mass loss over the azimuth to get the repulsive wind torque acting on the disk at each radius. Above a flat disk the wind loss is symmetrical in azimuth and its torque vanishes. But when the flat geometry is disturbed a little some regions of the disk surface get more illuminated than others, the wind gets stronger there and the integral of the torque does not vanish any more. Depending on the flow geometry and the height of the sonic point where the interaction between the flow and the underlying corona/disk system ends the wind torque enlarges the inclination and precession of the disk rings. On the other side, viscosity tries to smooth out any deviation from the flat disk geometry. But for small inclinations the viscous torque increases linearly while the wind torque increases non-linearly with increasing inclination. Thus any little disturbance grows until a new balance between all acting torques is reached. The disk remains warped.

If there are several states for the torque balance the disk shape will jump between them whenever a disturbance is large enough. The wind model includes a little spectrum of balance solutions. This is consistent with the observed strong variations of the longperiodic behaviour including total drops of the X-ray intensity for several cycles in 1983 (Parmar et al. 1985) and 1993 (Vrtilek et al. 1994) although the accretion went on as the optical data show (Delgado et al. 1983).

3. The geometrical structure of the disk

Figure 1 shows the solution of the torque equation for the Eulerian angles of inclination β and precession γ where we set the tilt of the inner disk region to be 4°. This solution belongs to a disk of radius $1.7\, 10^{11}$ cm which is 82% of the Roche radius corresponding to the radius which is necessary for the transfer of angular momentum back to the orbital motion (Paczyński 1977, Papaloizou & Pringle 1977).

β and γ are a solution of the torque equation of Bardeen & Petterson (1975) where we have replaced the Lense-Thirring effect by our derived coronal wind torque (Schandl & Meyer 1994). Papaloizou & Pringle (1983) have pointed out that these torque equations do not conserve the angular momentum. But as we found out their "naive approach" and the Bardeen & Petterson equations are the same in the case of small inclinations. Thus for our conditions each set of equations is useful.

While β is nearly the same at each radius, γ changes by more than 270°. Both features do not depend very much on the details of the wind model. E.g. the strong decrease of γ down to a minimum near the outer disk radius is dominated by the Coriolis force at inner radii and the tidal force at the outer disk. Thus warped disks look model independently like spirals with a turning point at the outer radii. This is shown in Fig. 2 where γ is shown in polar coordinates (dotted line). This line describes the intersection between the warped accretion disk and the orbital plane. The adjacent spirals show the intersections of the upper (solid line) and lower (dashed dotted line) disk surfaces with

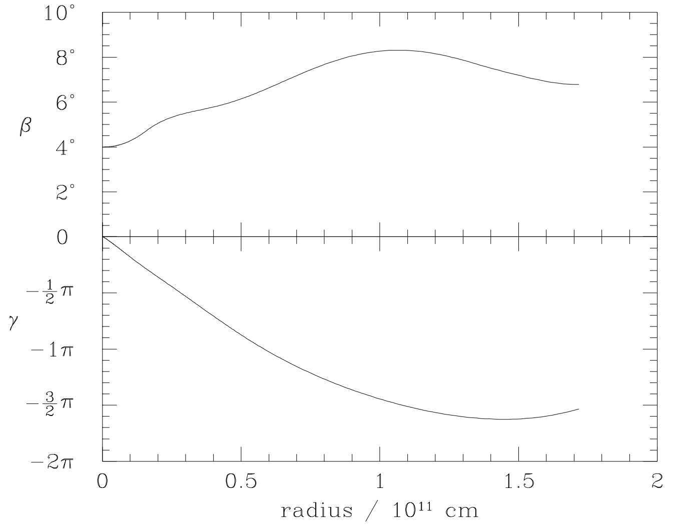

Fig. 1. The Eulerian angle of the tilt β and the precession γ as a solution of the torque equation (Schandl & Meyer 1994) with the parameters shown in table 1.

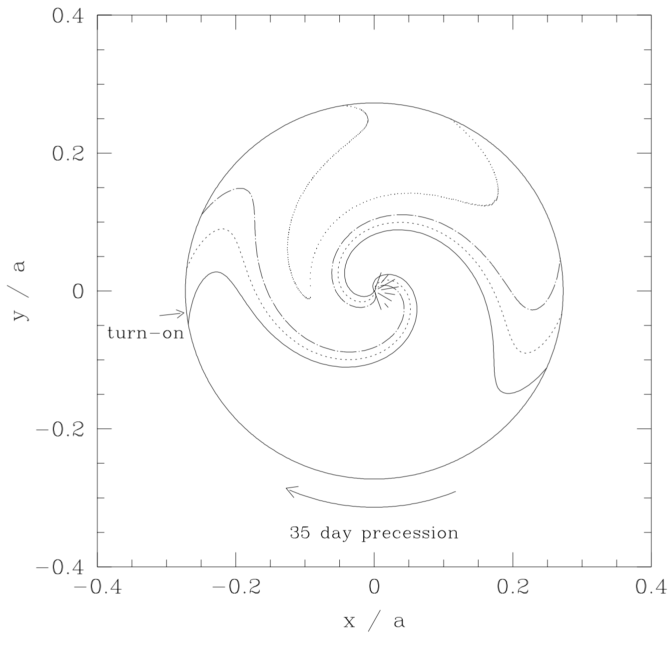

Fig. 2. The warped accretion disk from the top in units of the separation a. The spirals indicate the intersection between the disk and the orbital plane (solid line - upper surface; dashed dotted line - lower surface; dotted line - disk center). The region inside the dotted area rises by more than 8.5° indicating that it covers the central X-ray source if it intercepts the line of sight to the earth. At the end of this covering the turn-on is marked. The stripes at the inner disk show the phases where the optically thick part of the corona covers the source.

the orbital plane. For this we assumed a constant opening angle of the disk of $2 \cdot z_{\rm d}/r = 4°$.

The inclination of the system is assumed to be 81.5°. During the 35 day precession of the disk the line of sight from the observer to the central neutron star lies on a cone whose opening angle is the inclination. It intersects the upper surface of the disk at the dotted line. Whenever the line of sight crosses this dotted line the observer looks against the disk. At all other phases of the 35 day cycle the observer looks over the disk surface.

Above the inner disk there is the optically thick part of the corona. Because of the tilt of the inner flat part of the disk there are some phases of the 35 day cycle where the corona covers the central X-ray source indicated in the inner part of Fig. 2.

Figure 3a shows the upper and lower boundaries of the disk and the angle of declination where the optical depth of the corona equals unity. The orbital plane corresponds to the declination 0. With this figure it becomes clear that the inner Lagrangian point gets never illuminated directly. Thus a such tilted and twisted accretion disk cannot undergo periodic mass transfer as proposed by Crosa & Boynton (1980). Their model uses a much more tilted but far less twisted disk shape to illuminate the inner Lagrangian point temporarily.

In Fig. 3a the line of sight to the observer has to be drawn at constant declination of 8.5°. It gives an idea of the X-ray light curve of the model plotted in Fig. 3b. Here we calculated the observed relative X-ray intensity $F_{\rm x,rel}$ of the neutron star. During the eclipses by the companion and the covering of the neutron star by the disk (dotted region in Fig. 2) we set $F_{\rm x,rel} = 0$. Otherwise we set $F_{\rm x,rel} = {\rm e}^{-\tau}$, where τ is the optical depth in the corona.

One can see that our coronal model yields a density which is still too small compared to the observations though of correct order of magnitude. A density (and optical depth) which is 2 to 3 times higher would result in a total drop of the intensity $F_{\rm x,rel} = {\rm e}^{-\tau}$.

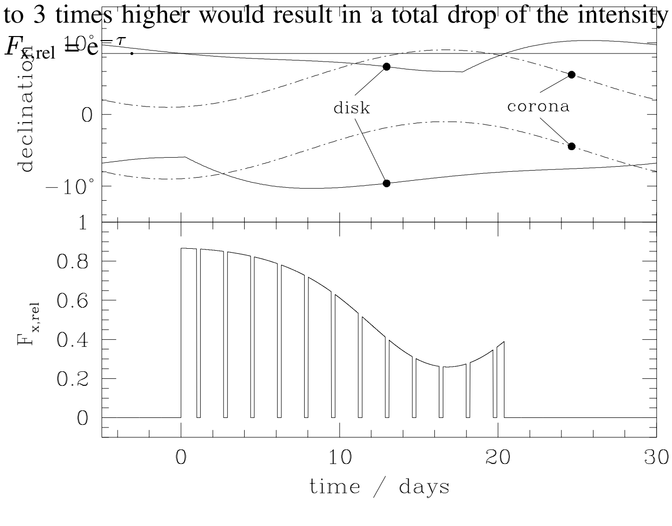

Fig. 3. One 35 day cycle is drawn. The upper picture (3a) shows the shadow belts of the disk (solid) and the corona at $\tau = 1$ (broken). The straight line at 8.5° is the line of sight to the earth. In the lower figure (3b) the calculated X-ray light curve including the eclipses is plotted.

The cause for this shortcoming might well lie in our simple treatment of the magnetospheric boundary where we have put the density to zero inside because the main contribution to the optical depth occurs in the region outside. But the infalling material in the magnetosphere rises from the orbital plane and illuminates the inner disk surface from above by scattering of X-rays. Because the corona is optically thin in vertical direction, this additional amount of illumination is of the same order as the 3% irradiation of scattering inside the corona. Such an effect might lead to the observed total obscuration at turn-off.– Note that because the outer regions are not affected by this process we do not expect any relevant change for our coronal wind at $r \geq 10^{10.2}$ cm and thus the results of our model with respect to the warp of the disk remains unchanged.

The increase later in the cycle corresponds to the observed short-on which ends due to the disk crossing the line of sight.

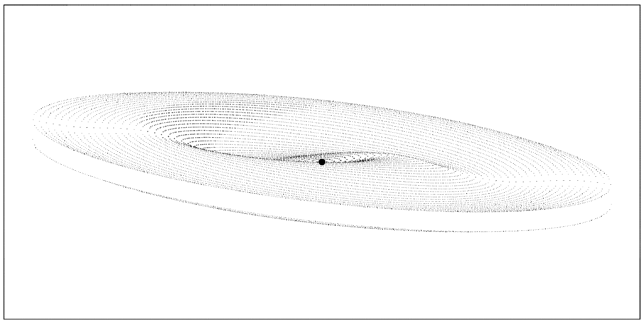

Fig. 4. The view to the disk at turn-on where the surface just opens the view to Her X-1. The bigger dots indicate the X-ray irradiated surface region.

The disk itself is plotted in Fig. 4 at turn-on. It makes clear that at this phase of the cycle where the direct light from the center is not jet seen the corona scatters the light to the observers. They measured an X-ray intensity which is a few percent of the main-on signal with the same spectrum but mostly not pulsed (Becker et al. 1977, Davison & Fabian 1977, Pravdo et al. 1979). They concluded that this must be light scattered by an extended corona. The scattering region has to be larger than 10^{10} cm in order to smear out the pulses by light travel time effects. This is of the same order as the diameter of our simulated optically thick corona. The simulated fraction of 3% radiation scattered in this corona reproduces the observations.

We point out the illuminated surface of the disk itself also scatters X-rays because its albedo is non zero. For this Fig. 4 indicates the illuminated and observable region by bigger dots. This scattered light which is of the order of a few percent may be the origin of a non covered component of the iron emission line which is generated by scattering at cold matter during a preeclipse dip as observed by Choi et al. (1994).

Thus the model reproduces the general features of the X-ray light curve of Her X-1. To simulate the detailed dip structure we investigate now the effects of the accretion stream on the disk.

4. Modelling the effects of the accretion stream on the disk

At the beginning we want to emphasize that the interaction of the accretion stream and the disk takes place at a frequency which is the sum of the observed orbital motion and the retrograde precession. This is the synodic period of 1.62 days. Considering the processes inside the system we have to use this period.

4.1. The accretion stream properties

The accretion stream starts at the Lagrangian point with about the sound velocity. For this the temperature is assumed to be the stellar temperature of about 7000 K (Gerend & Boynton 1976) yielding a sound velocity of $c_{\rm s,HZ} = 10^6$ cm/sec.

As mentioned above the observation of the orbital period change suggests a mass loss of the system due to the coronal wind of about three times the accretion rate of the neutron star $\dot{M}_{\rm acc} = 10^{17.3}$ g/sec. Thus we find for the mass flow in the stream $\dot{M}_{\rm s} = 10^{17.9}$ g/sec.

The cross-section of the stream is estimated as (see e.g. Meyer & Meyer-Hofmeister 1983)

$$A_0 = \frac{c^2_{\rm s,HZ}\, P^2_{\rm orb}}{2\pi\, k} \qquad (1)$$

where

$$k^2 = \left(\frac{m_1}{x_{\rm L}^3} + \frac{m_2}{(1-x_{\rm L})^3} - 1\right)\left(\frac{m_1}{x_{\rm L}^3} + \frac{m_2}{(1-x_{\rm L})^3}\right) = 54, \qquad (2)$$

$m_1 = M_1/(M_1{+}M_2), m_2 = 1-m_1, x_{\rm L} = r_{\rm L}/a$ and $r_{\rm L}$ is the distance between the primary (Her X-1) and the inner Lagrangian point. We find $A_0 = 10^{20.6}$ cm^2.

For simplification we assume that it keeps its width in the orbital plane and reduces its vertical extension proportional to r, the radial distance to the neutron star, during its fall to the accretion disk. That is we assume a free and supersonic fall of the stream particles neglecting their interaction.

This description concerns the stream central region which can explain both dip features. To simulate the particular orbital phases of the turn-on a more extended stream with low densities in its outer parts will be necessary. Thus we consider the stream as consisting of two parts: The inner high density region where A is the cross-section and in which nearly all the mass flows and an extended stream with low mass flow.

4.2. The geometry of the stream-disk-interaction

As a consequence of the warped shape of the disk the accretion stream strikes the disk surface at a particular radius that depends on the synodic orbital phase (Figs. 5 and 6a). Note that the impact region (hot spot) jumps on the surface. Further Fig. 5 shows that the accretion stream in the orbital plane is not illuminated directly by the X-ray source except at phases where

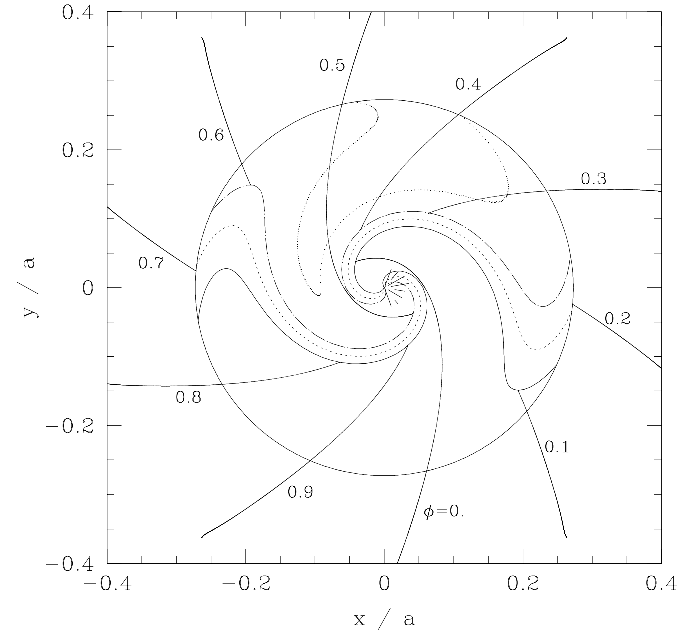

Fig. 5. The disk and the accretion stream for different orbital phases. The companion is not shows but the streams start at the inner Lagrangian point and end where they penetrate into the disk. The lateral extent of the stream is left out, too.

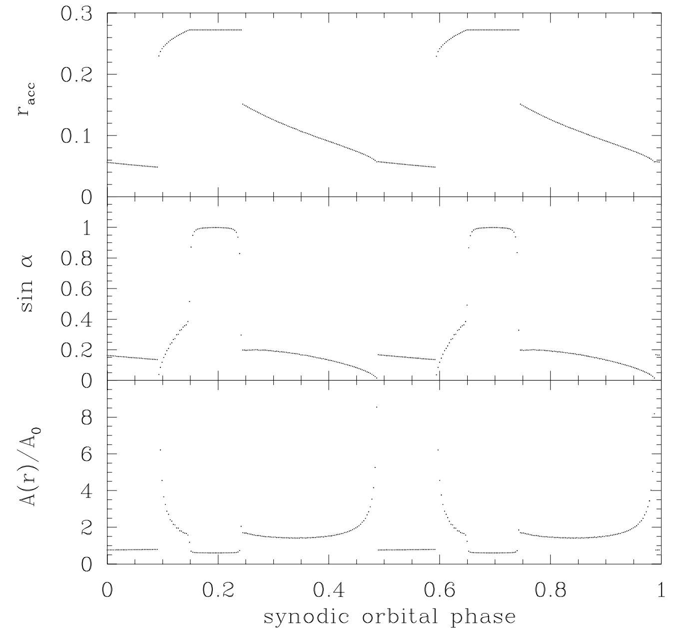

Fig. 6. The upper figure (6a) shows the accretion radius of the penetrating stream for different synodic orbital phases. The sine of the angle between the stream direction and the local plane of the disk surface is plotted below (6b). The lower picture (6c) shows the impact area in units of the initial stream cross section at the inner Lagrangian point. The phase is fixed except for an additional constant.

it strikes the very inner region (here at synodic orbital phases around 0 and 0.5) and that only just before the impact.

Figure 6b shows the sine of the angle α between the flow direction and the tangent of the disk surface in the same direction. Thus the area where the accretion stream center strikes the disk is $A(r) = (r/r_{\rm L})\, A_0/\sin\alpha$. In Fig. 6c $A(r)/A_0$ is plotted. When the accretion stream strikes the disk nearly tangentially ($\sin\alpha = 0$) the area gets very large. However, for the orbital phases of interest we can take a nearly constant area $A = A(r) = 2A_0 = 10^{20.9}$ cm^2 and $\sin\alpha = 0.15$.

4.3. The surface densities

Assuming further on that the flow velocity has approached the free fall velocity $v_\phi = (GM/r)^{1/2}$ we can compare the contribution of the mass flow in the stream to that in the disk. The time where the disk matter runs past the stream cross-section is about $dt = \sqrt{A}/v_\phi$. The disk surface density is $\Sigma_{\rm d} = \dot{M}_{\rm acc} v_\phi / 2\pi r\, c_{\rm s}^2$ where $c_{\rm s} \simeq 10^6$ cm/sec is the sound velocity at disk temperature 10^4 K. We get

$$\frac{\Sigma_{\rm s}}{\Sigma_{\rm d}} = \frac{\dot{M}_{\rm s}\, dt}{A\, \Sigma_{\rm d}} = \frac{\dot{M}_{\rm s}}{\dot{M}_{\rm acc}} \frac{2\pi\, r}{\sqrt{A}} \frac{c_{\rm s}^2}{v_\phi^2} \simeq 10^{-1.3}\, r_{11}^2 \tag{3}$$

where the superscript of r_{11}^2 shows the dependence of the result on the radius and the subscript describes the logarithm of the reference length. – Thus the contribution of the stream to the disk surface density is about twenty times smaller than of the disk matter itself.

4.4. The penetration depth of the stream into the disk

Because the flow velocity vertically to the disk $v_{\rm z} = v_\phi \sin\alpha \simeq 10^{6.8}$ cm/sec is highly supersonic the collision with the disk matter which itself moves with supersonic velocity produces shocks. We want to discuss two different scenarios – strong shocks with and without cooling.

The gas of the accretion stream penetrates into the disk until its shock pressure p_2 compares to the disk pressure $p_{\rm d}$. For strong shocks we find $p_2 = f\, \rho_1\, v_{\rm z}^2$ where ρ_1 is the density of the accretion stream before the shock and f equals 1 for strong isothermal shocks and 3/4 for strong adiabatic shocks. Setting $f = 1$ for an estimation we find

$$\frac{p_2}{p_{\rm d}} = \frac{\rho_1\, v_{\rm z}^2\, 2H_{\rm d}}{\Sigma_{\rm d}\, c_{\rm s}^2} = \frac{\dot{M}_{\rm s}}{\dot{M}_{\rm acc}} \frac{4\pi r\, H_{\rm d}}{A} \sin^2\!\alpha = 10^{-0.3}\, r_{11}^{5/2}. \tag{4}$$

Thus the stream penetrates deep down to the midplane of the disk but will probably not go through it.

4.5. The involved disk matter

Now we estimate the rate at which matter in the disk passes through shocks. Assuming roughly a constant vertical temperature distribution the stream penetrates until the density is half the central density (Eq. 4). Therefore about 1/4 from the whole surface density has to be considered:

$$\frac{\dot{M}_{\mathrm{shocked}}}{\dot{M}_{\mathrm{acc}}} = \frac{\frac{1}{4}\Sigma_{\mathrm{d}}\, v_\phi \sqrt{A}}{\dot{M}_{\mathrm{acc}}} = \frac{1}{4}\,\frac{v_\phi^2}{c_{\mathrm{s}}^2}\,\frac{\sqrt{A}}{2\pi\, r} = 10^{1.3} r_{11}^{-2}. \tag{5}$$

Thus about five times more disk matter is involved than what arrives in the accretion stream.

5. The spray and the preeclipse dips

Assuming that nearly all the kinetic energy of the accretion stream perpendicular to the disk surface, $\rho_1 v_z^2$, is converted into heat and that the shock takes place in an optically thin region, the gas cools down very quickly because the cooling timescales are very short compared to the dynamical time. If no effective cooling is possible the hot shocked gas expands with a velocity comparable to v_z. Because of an overall velocity of about v_ϕ the expansion has an opening angle comparable to α.

This corresponds to the simulations of Dgani et al. (1989) of the accretion stream striking the outer rim of a flat disk excluding strong cooling. They found a reflected jet of the order of one percent of the flow in the stream. But as Rozyczka & Schwarzenberg-Czerny (1987) argued a jet will not form in the case of effective cooling. In this case the whole stream belongs to the disk at once.

The difference to our impact geometry is that their stream hits the disk rim at the midplane. Into a warped disk the stream penetrates from its surface. Thus the disk matter at the disk surface runs against this obstacle with Kepler velocity at an angle δ between its velocity and the shock front which depends in detail on the penetration depth of the stream at this place (see Fig. 7). Because the velocity component parallel to the shock remains unchanged and the perpendicular component gets smaller the shock 'refracts' the flow direction of the matter which gets a velocity component perpendicular to the orbital plane forming a spray. Especially we will show now that it occurs independently of the importance of cooling.

5.1. The flow direction of the spray

To find a rough estimation of the possible angles of refraction we consider the velocities in the coordinate system where the shock front is at rest. The velocity component tangentially to the front remains unchanged, while the perpendicular component slows down by a factor of about 4 assuming $\gamma = 5/3$ in strong adiabatic shocks. If there is effective cooling the shock becomes isothermal and the vertical velocity component changes by a factor of $(c_{\mathrm{s}}/v_{\mathrm{z}})^2 = 10^{-1.6}$ and thus this velocity gets negligible.

Assuming an angle between the disk matter and the shock front in the disk plane (x-y-plane) of 45° (see Fig. 5) the shocked gas follows nearly the tangent of the front if it does not collide with other disk matter. But this is the case only for matter at the disk surface which leaves the disk plane with its vertical velocity component forming the spray.

At an angle δ between the disk surface matter and the shock front in the x-z-plane (Fig. 7) we find refraction angles between

Fig. 7. This figure sketches the refracting geometry of the shock front for disk matter running against the penetrating accretion stream. Depending on the angle δ and the effectiveness of cooling the matter at the disk surface sprays upwards.

the spray and the disk plane ξ of up to 40° in the isothermal case and up to 33° in the adiabatic case. This is both at $\delta \simeq 50°$. For smaller and larger δ the refraction of the shocked gas results in a smaller ξ. Thus for further calculations we take a mean value of $\xi = 20°$ which yields a vertical velocity of the spray of the order of v_{z}.

5.2. The preeclipse dips

Looking at Fig. 5 the stream strikes the upper surface of the disk (which the observer looks at) for almost half the synodic orbit. At the other times it strikes the lower surface or the disk rim. Striking the upper surface the spray flows upwards. During this time it is possible that the spray covers the central X-ray source for the observer. In this case we expect a partial and time variable intensity drop with cold matter absorption features in the spectrum as it is observed during preeclipse dips.

Choi et al. (1994) observed 21 preeclipse dips with Ginga. They found a time variability of 30 sec where the intensity changes up to a factor of 5. Assuming absorption cross-sections of Morrison & McCammon (1983) they found column densities around 10^{23} H atoms cm^{-2} (in the range $10^{21.2}$ cm^{-2} to $10^{24.1}$ cm^{-2}). Reynolds & Parmar observed with Exosat in three dips a mean value of $N_{\mathrm{H}} = 10^{23.7}$ cm^{-2} where Giacconi et al. (1973) derived typical column densities of 10^{23} cm^{-2} with Uhuru. Using a dip duration of $\Delta t = 4$ hrs we can now estimate the extension of the spray to be

$$d_{\mathrm{spray}} = 2\pi\, r\, \frac{\Delta t}{P_{\mathrm{orbit}}} = 0.6\, r\, \Delta t_{4\mathrm{hr}}. \tag{6}$$

Assuming a vertical spray velocity of the order of v_z one obtains for the mass flow in the spray

$$\frac{\dot{M}_{\rm spray}}{\dot{M}_{\rm acc}} = \frac{\mu\, m_{\rm p}\, N_{\rm H}\, v_{\rm z}\, d_{\rm spray}}{\dot{M}_{\rm acc}} = 10^{-0.5}\, r_{11}^{1/2}\, N_{\rm H23}\, \Delta t_{\rm 4hr}. \quad (7)$$

In comparison to the estimated involved disk matter we get a fraction of

$$\frac{\dot{M}_{\rm spray}}{\dot{M}_{\rm shocked}} = 10^{-1.8}. \quad (8)$$

Thus only a few percent of the shocked disk matter is necessary to reproduce the observed dip structure.

Another important consistency of our model and the observations are the times and phases where the dips occur. The stream penetration region has to lie on the upper disk surface and additionally near the line of sight between the observer and the neutron star. This happens during main-on at orbital phases just before the eclipses as it is observed. The marching of the dips to progressively earlier (1.7 day orbital) phases during the 35 day cycle is a pure geometrical effect (getting obvious in Fig. 5).

To simulate the times of the dips we assume that the spray is refracted at the penetrating accretion stream into a direction nearly parallel to the shock and thus following the stream free fall flow direction in the orbital plane. The additional vertical velocity component is the time integral

$$v_{\rm z}(t) = v_{\rm z} - \int_{t_{\rm impact}}^{t} \frac{G\, M\, z(t')}{r^3(t')}\, dt'. \quad (9)$$

At a height $z(t) = r\,\sin(8.5°)$, corresponding to the inclination of the system, we can check now whether the spray of the observed width of $d_{\rm spray}$ covers the neutron star. The simulated dips are shown in the X-ray light curve in Fig. 8a.

The simulated period of the dips of about 1.66 days calculated from Fig. 8b reproduces the observed preeclipse dip occurrence (Giacconi et al. 1973) very well. This includes the preeclipse dip Jones & Forman (1976) observed during the low state (at $\phi_{35} = 0.6$) at orbital phase 0.56.

Note that this period actually compares to the synodic orbital period but is caused by a quite different mechanism in our model.

5.3. Optical observations of the spray

The spray has to consist of gas which is cold enough to make cold absorption features in the spectrum. Karitskaya et al. (1986) and Howarth & Wilson (1983) have observed emission in the optical and UV of blobs of a temperature of $T = 10^{4.4}$ K and densities of $n_{\rm e} = 10^{13.3}\,{\rm cm}^{-3}$. The phases of the appearance of the blobs correspond to half the synodic period (Karitskaya et al. 1986) and seem to be related to the interaction between the accretion stream and the disk *rim*.

Bochkarev and Karitskaya (1989) connected these blobs with the Crosa & Boynton (1980) model of periodic mass transfer. In contrast to their model the accretion stream in our model is stationary. But the interaction with the disk *rim* takes place at the same period. Thus the observed blobs fits into both models.

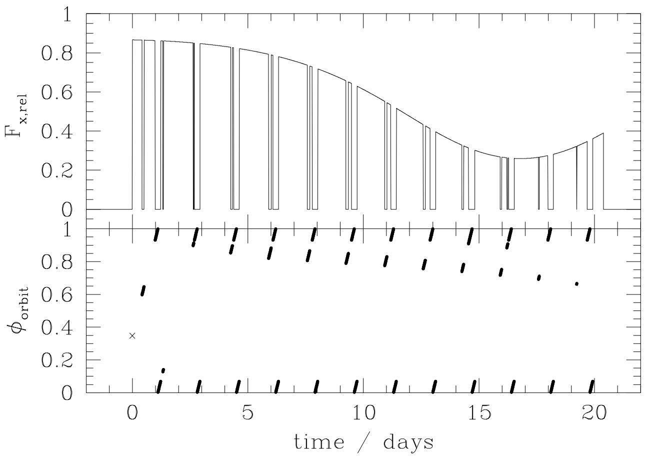

Fig. 8. The calculated X-ray light curve including the anomalous and preeclipse dips using a less extended accretion stream (8a). The turn-on is marked by a cross in the lower picture where the orbital phases of the dips and eclipses are shown. This kind of representation clarifies the marching back of the preeclipse dips in orbital phase.

A difference between the periodic mass transfer model and the coronal wind model is the matter doing the preeclipse dips. Because in the first model the blobs are exclusively generated at the phases of mass transfer corresponding to the above mentioned observations this gas is responsible for the preeclipse dips. This results in a blob generation at progressing earlier orbital phase with progressing later 35 day precession. That is, the time between their generation and their flow through our line of sight gets longer during the 35 days. Because the blobs evolve and fill a large volume (Bochkarev and Karitskaya 1989) this should be observable in a changing dip behaviour – longer and less deep.

In the coronal wind model this is not the case. Here the spray responsible for the preeclipse dips is generated just before the dip. Thus we should always observe a 'young' spray. Because of the small angle α this spray is presumably not observable in the optical because in projection it runs in front of the disk.

6. The disk thickening, the anomalous dips and the turn-ons

6.1. The disk thickening

The hydrostatic layering of the accretion disk matter gets disrupted where the stream impacts. The turbulent motion of the shocked gas and the additional energy input by the stream cause an increase of the disk thickness. For an estimation we compare the disk energy and the energy added by the stream.

$$\eta = \frac{\Sigma_{\rm s}\, v_{\rm z}^2}{\Sigma_{\rm d}\, c_{\rm s}^2} = 10^{0.3}\, r_{11} \quad (10)$$

(see Eq. 3). Thus the inner energy of the disk increases by a factor $1 + \eta$, and the disk scale height $H_{\rm d}$ therefore grows by a factor $\sqrt{1+\eta}$. Because of cooling effects this factor is an upper limit for the disk thickening.

Because of the orbital motion of the matter the disk gets thick along circles until the smoothing viscosity and thermal relaxation have restored the hydrostatic order. This will last about one dynamical timescale which compares to the Kepler period. Thus we assume a thickening which gets smoothed out exponentially with exp $(-\phi)$.

6.1.1. The anomalous dips

The anomalous dips occur only just after turn-on and only at orbital phases around 0.2 and 0.7. Giacconi et al. (1973) observed a dip at $\phi = 0.23$ after a turn-on at $\phi = 0.68$, Davison & Fabian (1977) found a dip at $\phi = 0.6$ with turn-on phase 0.7 suggesting a marching of the anomalous dips. Alltogether anomalous dips occur at the same phases as the turn-on itself.

In our model the disk ring at a radius $r_{\text{turn-on}} = 6\,10^{10}$ cm causes the turn-on. Thus looking marginally over the disk surface our view is most sensitive for disk processes at this radius.

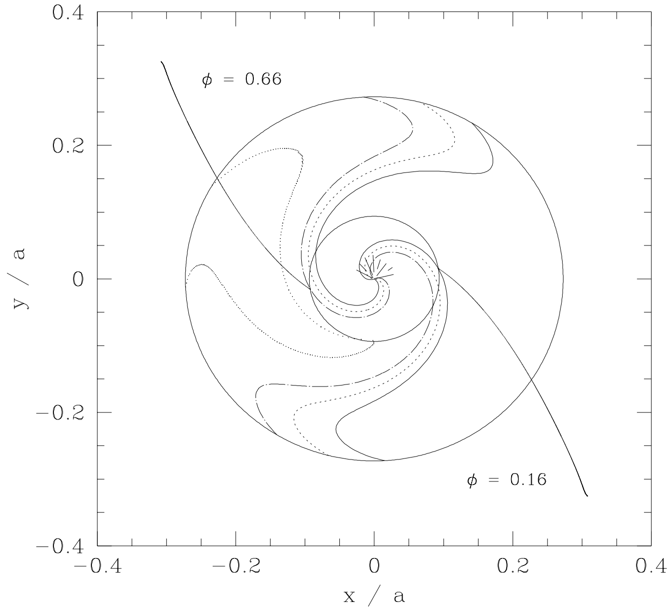

Fig. 9. This is the disk at turn-on with two accretion streams at those synodic orbital phases where the disk ring doing the turn-on is impacted. These are the two possible phases for the occurrence of the turn-on and the anomalous dips.

During each orbit there are two times when the accretion stream strikes the disk at this radius. Fig. 9 shows that this is around phases $\phi = 0.16$ and $\phi = 0.66$. As discussed above now the disk ring gets thicker and covers the X-ray source again until the accretion stream has moved on the disk surface. This reproduces an anomalous dip: It occurs only just after turn-on, because later the line of sight to the X-ray source is far above the disk. It occurs only at two fixed phases because of the impact geometry of the accretion stream. This is about one half (and perhaps two halfs) of the synodic orbit after the phase of the turn-on and reproduces the marching of the dips relatively to the turn-on. And of course the spectrum is the same as at turn-on, because it is the same disk matter covering the source.

To simulate the anomalous dips we assumed a thickening of the disk rings of $d_0\,\mathrm{e}^{-(\phi-\phi_{\text{acc}})}$ at the radii involved which are in the interval $r_{\text{acc}} \pm \frac{1}{2}\sqrt{A}$ (see Fig. 6). Thus we include only the dense stream center neglecting firstly a more extended shape of the stream. ϕ_{acc} is the orbital phase of the stream penetration, d_0 is the disk thickening at the stream penetration region. Large values of d_0 results in many anomalous dips, for too small values no dip occurs. To get two dips we have to set $d_0 = 0.3° = \frac{1}{5}H_{\text{d}}$, to get only one dip we set $d_0 = 0.2° = \frac{1}{8}H_{\text{d}}$. Comparing this with the result of Eq. (10) we find for the calculated upper limit of the thickening at $r_{\text{turn-on}}$

$$d_{0,max} = H_{\text{d}}^{+} - H_{\text{d}} = (\sqrt{1+\eta} - 1)\,H_{\text{d}} = 0.48\,H_{\text{d}} \qquad (11)$$

which corresponds to our simulation.

Figure 8 shows the calculated anomalous dips in the X-ray light curve. They occur at orbital phases 0.6 and 0.15.

6.2. The orbital phases of the turn-on

As Fig. 4 supposes the turn-on occurs in our model when the precessing accretion disk clears the line of sight to the central X-ray source. The rise of the signal in less than 2 hours (Giacconi et al. 1973) and the energy dependent absorption in the X-ray spectrum (Becker et al. 1977) suggest the connection with the cold disk matter.

The turn-on occurs in the intervals of the orbital phases 0.19 - 0.3 or 0.63 - 0.75 (e.g. Giacconi et al. (1973) observed 9 turn-ons, Davison & Fabian (1977) 3). Getting obvious in Fig. 9 the stream strikes the disk inside the turn-on radius for about 0.1 orbital period after the simulated anomalous dip phases. Because the turn-on radius is not involved we do not expect any thickening there during this time. Now either (first case) the undisturbed region covers the X-ray source further on or (second case) the turn-on occurs.

Afterwards the impact region jumps to the outer radii, the rim and then moves inwards again. To avoid a turn-on at the corresponding orbital phases in the first case the turn-on region has to get thicker and thus must be involved in the stream penetrating process. More precisely the thickening has to grow from small values until the stream center itself hits the critical radius producing a temporary peak of the thickening: A moderate growth of the thickening results for the second case in a persistent on-state and the peak at the stream center impact causes the following anomalous dip.

This behaviour is sketched in Fig. 10 where the temporal behaviour of the vertical extend of the disk is shown (a detail of Fig. 3 around turn-on). Drawn are the disk height without any stream interaction, with included thickening due to the stream center and due to the extended stream.

In the simulation above only the dense stream center is included. Therefore the turn-on occurs at some orbital phase

Fig. 10. The vertical disk extension around turn-on. The solid line corresponds to a disk with no stream interaction. The additional dashed thickening shows the effect of the interaction with the central dense accretion stream and the dotted marked thickening is caused by the interaction with an extended stream. An extended stream causes the anomalous dips and turn-ons exclusively around orbital phase 0.2 or 0.7. Especially looking to the scatter in the precession period of up to 10% (Ögelman et al. 1985) the possible orbital phases of turn-on are independent on this: The random walk shifts the solid line of the undisturbed disk horizontally, but the additional thickening remains fixed to the orbital phase – it moves only up or down in the figure.

(here $\phi = 0.35$) which is not determined by the stream/disk interaction. But in the case of an extended stream the disk thickness will be increased jet at this phase and the turn-on occurs not until the end of the following anomalous dip, this is at phase $\phi = 0.66$. The anomalous dip at $\phi = 0.15$ remains unchanged by this effect of an extended stream.

Although this is an idealized proposal explaining the observed turn-on behaviour it indicates that the accretion stream would be extended. A dense stream center as described in the sections above together with a more extended stream of lower density could reproduce all the observations.

In this context the observations of Pravdo et al. (1979) get very interesting. They observed a partial onset about one orbit before the turn-on. During this intermediate state the spectrum shows cold matter absorption features in contrast to the low state before and the high state afterwards. Pulsations were present. Even some signal reduction at the typical anomalous dip phase 0.6 may be suggested in their observations. – This shows that the observations do not demand such a strictly idealistic disk thickening behaviour as described above.

Finally we want to consider the relation between the two observed turn-on phases. The first phase interval is centered at phase 0.225 and the second at 0.685 (Giacconi et al. 1973). The phase difference is not 0.5 as it could be expected from symmetry arguments. If this is due to the Kepler motion of the thickening through the disk, the time difference of $0.04 P_{\rm orbit}$ corresponds to half a Kepler period which the gas at impact phase 0.225 has to circulate longer than the gas at the later impact in order to cross the line of sight (see Fig. 9). This would correspond to a turn-on radius of

$$r_{\rm turn-on} = \left(\frac{0.04}{\pi} \sqrt{GM}\, P_{\rm orbit} \right)^{2/3} = 10^{10.9}\,{\rm cm} \qquad (12)$$

which compares to the radius of $10^{10.8}$ cm obtained from the disk model.

7. Conclusions

The interaction between the accretion stream and the thin warped disk has been found to be the origin of the complex dip structure in the X-ray signal. The spray explains the spectral and time variable intensity structure of the preeclipse dips. The mass flow in the spray calculated from the column densities of cold matter observed during the dips can be generated by a few percent of the disk matter involved into the stream impact scenario. The disk shape resulting from the coronal wind model reproduces the occurrence times of these dips.

The anomalous dips are modelled by a temporal thickening of the disk region we look marginally over at turn-on. Considering the energy input by the stream we estimated a thickening of the correct order. The simulated orbital phases of the stream impact at the corresponding critical radius are the same as the observed phases.

To fit the discret orbital phases of the turn-on we need a more extended accretion stream to impact the critical radius progressively during the time between the possible turn-on phases. This makes the turn-on to be a zeroth anomalous dip.

I am grateful to Friedrich Meyer for checking the concept of this model, for the precious ideas for the estimates and for the detailed comments on the manuscript. I thank R. Staubert for calling my attention to the dip feature problem and M. Ruffert for helpful discussions about shocks.

References

Bardeen J.M., Petterson J.A., 1975, ApJ 195, L65 (BP)
Becker R.H., Boldt E.A., Holt S.S. et al., 1977, ApJ 214, 879
Begelman M.C., McKee C.F., 1983, ApJ 271, 89
Bochkarev N.G., Karitskaya E.A., 1989, Astr. and Sp. Sci. 154, 189
Boynton P.E., Crosa L.M., Deeter J.E., 1980, ApJ 237, 169
Choi C.S., Nagase F., Makino F., Dotani T., Min K.W., 1994, ApJ 422, 799
Crosa L.M., Boynton P.E., 1980, ApJ 235, 999
Davison P.J.N., Fabian A.C., 1977, MNRAS 178, 1
Deeter J.E., Boynton P.E., Miyamoto S. et al., 1991, ApJ 383, 324
Deeter J.E., Boynton P.E., Pravdo S.H., 1981, ApJ 247, 1003
Delgado A.J., Schmidt H.U., Thomas H.C., 1983, A&A 127, L15
Dgani R., Livio M., Soker N., 1989, ApJ 336, 350
Gerend D., Boynton P.E., 1976, ApJ 209, 562
Giacconi R., Gursky H., Kellog E. et al., 1973, ApJ 184, 227
Howarth, I.D., Wilson, B., 1983, MNRAS 204, 1091

Jones C., Forman W., 1976, ApJ 209, L131
Karitskaya E.A., Bochkarev N.G., Gnedin Y.N., 1986, Astron. Zh. 63, 1001
Katz J.I., 1973, Nature Phys. Sci. 246, 87
McCray R., Shull J.M., Boynton P.E. et al., 1982, ApJ 262, 301
Morrison R., McCammon D., 1983, ApJ 270, 119
Meyer F., Meyer-Hofmeister E., 1983, A&A 121, 29
Middleditch J., 1983, ApJ 275, 278
Middleditch J., Nelson J., 1976, ApJ 208, 567
Ögelman, H., Kahabka, P., Pietsch, W., Trümper, J., Voges, W. 1985, Space Science Reviews 40, 347
Oke J.B., 1976, ApJ 209, 547
Paczyński B.,1977, ApJ 216, 822
Papaloizou J., Pringle J.E., 1977, MNRAS 181, 441
Papaloizou J.C.B., Pringle J.E., 1983, MNRAS 202, 1181
Parmar A.N., Pietsch W., McKechnie S. et al., 1985, Nat 313, 119
Pravdo S.H., Becker R.H., Boldt E.A. et al., 1977, ApJ 215, L61
Pravdo S.H., Becker R.H., Bussard R.W. et al., 1979, In: Baity W.A. and Peterson L.E. (eds), X-Ray Astronomy, IAU/COSPAR, p. 219
Priedhorsky W.C., Holt S.S., 1987, Space Sci. Rev. 45, 291
Reynolds A.P., Parmar A.N., to be published in A&A
Rozyczka M., Schwarzenberg-Czerny A., 1987, Acta Astr. 37, 141
Schandl S., Meyer F., 1994, A&A 289, 149
Shakura N.I., Sunyaev R.A., 1973, A&A 24, 337
Tananbaum H., Gursky H., Kellog E.M. et al., 1972, ApJ 174, L143
Trümper J., Pietsch W., Reppin C. et al., 1978, ApJ 219, L105
Vrtilek S.D., Mihara T., Primini F.A. et al., 1994, ApJ 436, L9